Idle speed control of a direct injection spark ignition stratified charge engine

J. W. Grizzle[1,*,†], Julia Buckland[2] and Jing Sun[2]

[1]*Control Systems Laboratory, Electrical Engineering and Computer Science Department, University of Michigan, Ann Arbor, MI 48109-2122, U.S.A.*
[2]*Powertrain Control Systems Department, Ford Research Laboratory, 2101 Village Road, PO Box 2053, Dearborn, MI 48121-2053, U.S.A.*

SUMMARY

Idle speed control is investigated for a direct injection, spark ignition, stratified charge (DISC) engine equipped with an electronic throttle. Such engines can be operated in multiple combustion modes. When operating in stratified charge combustion mode, they are very different from conventional stoichiometric engines, creating new opportunities for improved speed control. With current after-treatment technology, simultaneous high fuel economy and emissions conversion efficiency cannot be achieved by operating the engine in a steady-state manner: it must be cycled between running ultra-lean (for fuel economy) and rich (to service the after-treatment system). An idle speed control system is designed to meet the considerable feedback control demands required by these new engines. Copyright © 2001 John Wiley & Sons, Ltd.

KEY WORDS: hybrid model; decentralized control; gain scheduling; switching control

1. INTRODUCTION

In recent years, many research and development activities have focused on achieving fuel economy improvements in spark ignition engines through reduced pumping losses [1–5]. One such technology is the direct injection stratified charge (DISC) gasoline engine [6]. Its recent introduction into the Japanese and European markets may extend to North America in response to increased environmental pressures and higher customer expectations for fuel economy and performance. In this type of engine, fuel is injected directly into the combustion chamber during the intake stroke to form a homogeneous mixture, or during the compression stroke to form a very heterogeneous mixture referred to as a stratified charge, or both. With stratified charge, the

---

*Correspondence to: J. W. Grizzle, Control Systems Laboratory, Electrical Engineering and Computer Science Department, University of Michigan, Ann Arbor, MI 48109-2122, U.S.A.
†E-mail: grizzle@umich.edu

engine can operate at overall air–fuel ratios up to $40:1$ or higher,[‡] thereby reducing pumping losses and increasing thermal efficiency. With its sophisticated combustion chamber and fueling system, and in combination with an advanced exhaust after-treatment system, a DISC engine has the potential of improving fuel economy and CO_2 emissions at an acceptable cost.

The implementation of DISC technologies, however, relies critically on the development of the control system to deliver the expected benefits. For a DISC engine, the task of maintaining optimal fuel economy operating conditions while satisfying emission and driveability constraints over a wide range of engine speed and load conditions is significantly more complicated than that for conventional port-fuel injected (PFI) engines. The following special features associated with DISC engines impose major challenges for control system development:

- Current DISC engines can operate in multiple combustion modes, characterized by charge composition, or equivalently, time of injection:[§] homogeneous (early injection), stratified (late injection), and even multiple injection. Because of significant differences in torque and emission characteristics, a distinct control strategy is required to optimize the engine operation in each mode. A control system has to determine dynamically not only in which mode the engine should be running according to engine and after-treatment device operating conditions and driver's input, but also effectively manage smooth transitions from one mode to another.
- A DISC engine has more control inputs than a conventional PFI engine. Besides the standard actuators such as throttle, fuel, spark, and exhaust gas recirculation (EGR), additional inputs, such as fuel injection timing and fuel system pressure, have significant effects on DISC engine performance, unlike PFI engines, where the effects are relatively minor. Flow control devices, such as a swirl control valve (SCV), are also necessary for proper mixing and charge formation. Furthermore, other advanced actuators, such as variable cam timing (VCT), continuously variable transmission (CVT) and boosting devices such as a variable geometry turbocharger (VGT) have been considered for DISC applications to realize the full benefits of lean operation. While these new actuators will enhance the overall system's capability to deliver good fuel economy and emissions, they have greatly increased system complexity thereby necessitating a system engineering approach to effectively manage this multi-objective, multi-variable problem.
- A DISC engine requires a special exhaust after-treatment system to meet emission regulations. At lean air–fuel ratios, the ubiquitous three-way catalyst (TWC) can effectively convert CO and HC in the exhaust gas to CO_2 and H_2O. The current NO_x removal technique is to place an additional TWC, referred to as a lean NO_x trap (LNT), after the existing TWC in the exhaust system. Since an LNT only traps NO_x, it must be periodically purged to maintain its level of conversion efficiency. By periodically operating the engine at a rich condition (in homogeneous mode), the trapped NO_x is purged and converted to N_2 by reductants such as CO, HC and H_2 [7–9]. The duration and frequency of the purge condition (rich operation of the engine), and obviously the control strategy for purging the LNT should be well optimized to achieve high fuel economy and low NO_x emissions. For example, for a DISC engine running in stratified mode, the LNT is typically purged by operating the engine slightly rich of stoichiometry for

[‡]The shape of the piston is designed to enhance air motion (swirl or tumble). The air motion, in combination with proper fuel injection timing, permits the creation of a concentrated, ignitable mixture around the spark plug [6].
[§]As noted earlier, charge composition depends directly on fuel injection timing.

approximately 2–3 s every 50 s. This purge cycle, if not properly managed, can create an undesirable torque disturbance and driveability problems. The LNT service requirement is one of the major challenges in developing a high-performance robust control system.

This paper addresses the problem of idle speed control [10–14] for a DISC engine equipped with an electronic throttle. As noted above, when operating with lean combustion, DISC engines are very different from conventional stoichiometric engines, creating new opportunities for improved speed control. In particular, air–fuel ratio is not constrained to a fixed value due to emission considerations and is free to vary over a fairly wide range. Consequently, fuel may be used as the primary fast torque actuator instead of spark. Spark can then be set to achieve best fuel economy and emissions. This is very similar to the diesel idle speed control problem, where fuel is the key control actuator for speed regulation. On the other hand, a key point with a DISC engine and LNT-based after-treatment system is that simultaneous high fuel economy and emissions conversion efficiency cannot be achieved by operating the engine in a steady-state manner. It must be continuously cycled between lean combustion and the rich purge condition [15]. This places considerable demands on the idle speed control system and sets the problem apart from conventional diesel idle speed control.

Due to the complex interactions of the DISC engine/after-treatment system, a hierarchical control architecture is assumed. Here, a supervisory engine controller determines the combustion mode and the corresponding fuel injection timing, as well as the desired set-points for air–fuel ratio, intake burned gas fraction, engine idle speed, etc., that meet the driver's demand and result in the best compromise between fuel economy and emissions. All other control features, including idle speed control, strive to meet the demands set forth by the supervisory controller. For the work presented here, it is assumed that the supervisory controller has been previously designed and all necessary commands from the engine control supervisor, including desired set-points, are known.

The paper is organized as follows. Section 2 presents the hybrid model of a DISC engine developed in Reference [16] and specializes it for an experimental 1.1 l, three cylinder, engine. Section 3 summarizes the idle speed control objectives for the engine, and motivates two different controller topologies to meet these objectives: a speed-dominant topology to control the engine during lean operation when air–fuel ratio is relatively unconstrained, and an air–fuel ratio-dominant topology when air–fuel ratio must be precisely controlled to a set-point. The controller designs for these two topologies are developed in Sections 4 and 5, respectively. Simulations demonstrating the ability of the designed controllers to reject load torque disturbances in both stratified and homogeneous combustion modes are also provided. Section 6 demonstrates the rapid completion of a purge cycle while idling, even under considerable load torque disturbances.

The model and control design will be presented in the continuous-time domain. Well-known results can be used to discretize the resulting controllers synchronously with engine crank-angle for implementation [12, 17, 18].

2. LEAN BURN ENGINE MODEL AND SENSORS

This section describes the mathematical model of the engine under study and the assumed sensor package. The model's structure is based directly on the DISC engine model of Reference [16], and reflects the multi-mode or hybrid nature of the system. The model's parameters correspond to an

experimental 1.1 l, three cylinder, engine. To simplify the development, the following assumptions will be made:

A1. For both homogeneous and stratified combustion modes, spark and fuel injection timings are set to achieve best fuel economy.
A2. The range of allowable air–fuel ratios varies continuously from a minimum of 12:1 to a maximum of 40:1. Homogeneous combustion is possible from 12:1 to 19:1 and stratified combustion is possible from 19:1 to 40:1.
A3. The changes in the intake manifold dynamics due to temperature variations can be handled through gain scheduling and robust control design, and thus a nominally constant temperature may be assumed.
A4. Fuel injection quantity is determined by the controller at a fixed point in the combustion cycle. Thus, even though best fuel injection timing will naturally vary as a function of engine conditions, the delay in torque production due to combined computation delay and fuel injection delay is constant in terms of crank angle.
A5. Other control issues such as fuel rail pressure, swirl control valves, model variability, etc. are ignored.

Assumption A1 is very natural for fuel economy reasons and simplifies the torque expressions used in the model. The framework proposed in this paper, however, can be easily extended to include spark and injection timings as active control variables, if necessary for emissions considerations. Assumption A2 means that, for some DISC engines, the results presented here may need to be supplemented to handle a disallowed range of air–fuel ratios, typically between the homogeneous and stratified regimes, where stable combustion without excessive soot formation is not achievable in either combustion mode. Assumption A3 simplifies the representation of the intake manifold dynamics and is straightforward to remove. Assumption A4 is reasonable from the perspective of real-time code execution. Assumption A5 narrows the scope of the problem for this work. The results presented here may need to be supplemented to account for these issues prior to implementation in a production vehicle. For example, the fuel rail pressure set-point must be scheduled appropriately such that the injector characteristics are linear at low load, idle conditions.

2.1. Engine model

With these assumptions, the air-charge, exhaust gas recirculation (EGR) and torque aspects of the engine are modelled as [16]

$$\dot{P}_i(t) = \frac{RT_i}{V}(W_{th}(t) + W_{egr}(t) - W_{cyl}(t))$$

$$\dot{m}_{bg}(t) = F_e(t)W_{egr}(t) - F_i(t)W_{cyl}(t) \tag{1}$$

$$\dot{N}(t) = \frac{30}{\pi J_e}(\mathcal{T}_i(t-d) + \mathcal{T}_{fric}(t) - \mathcal{T}_{load}(t))$$

where P_i is the intake manifold pressure (kPa); R is the ideal gas constant; T_i is the intake manifold temperature (K); V is the intake manifold volume (l); W is a mass flow rate (g/s), with subscripts th, egr and cyl representing electronic throttle, EGR and into-cylinder, respectively; m_{bg} is the mass of burned gas in the intake manifold (g); F_i and F_e are the burned gas fractions of the intake

and exhaust manifolds, respectively; N is engine speed (rpm); J_e is engine inertia (Nm s^2) and $\mathcal{T}$ is torque (Nm), with subscripts i, fric and load representing the indicated, combined mechanical friction and pumping loss, and load torques, respectively. d represents the combined computation and combustion delay[¶] (s) discussed in Assumption A4, which for this work corresponds to one engine revolution.

These equations are completed by the following expressions:

$$W_{cyl} = \alpha(N) + \beta(N)P_i$$

$$\mathcal{T}_i = a_0(N)(1 - F_i)W_{cyl} + a_1(N)W_f$$

$$\mathcal{T}_{fric} = f(P_i, N)$$

$$F_i = \frac{m_{bg}}{m_i}$$

$$m_i = \frac{V}{RT_i}P_i$$

$$d = \frac{60}{N}$$

$$J_e = 0.14$$

$$\frac{RT_i}{V} = 30$$

(2)

where W_f denotes the fuel flow rate (g/s) and m_i corresponds to the mass of gas in the intake manifold (g). The various functions in the model are determined by regression of engine mapping data. Figure 1 depicts the cylinder mass flow. Figures 2 and 3 depict the functions for indicated torque. Since the indicated torque depends strongly on the combustion mode, there are two values for each of a_0 and a_1, with the superscripts S and H differentiating the stratified and homogeneous combustion modes. Figure 4 depicts the friction torque.

The mass air flow rate through the electronic throttle valve, W_{th}, and the mass exhaust gas flow rate through the EGR valve, W_{egr}, are modelled with standard orifice flow equations [6] and any actuator dynamics have been ignored. Here, it is further assumed that both the electronic throttle and the EGR valve have been feedback linearized via pre-compensation and hence can be represented by a model of the form

$$W_{act} = \text{sat}_b^a(W_{act}^{des}) = \begin{cases} a & W_{act}^{des} \leqslant a \\ W_{act}^{des} & 0 < W_{act}^{des} < b \\ b & W_{act}^{des} \geqslant b \end{cases}$$

(3)

[¶]d includes the time between induction and torque production, including computational delay. It is included in (1) rather than (2) for mathematical convenience.
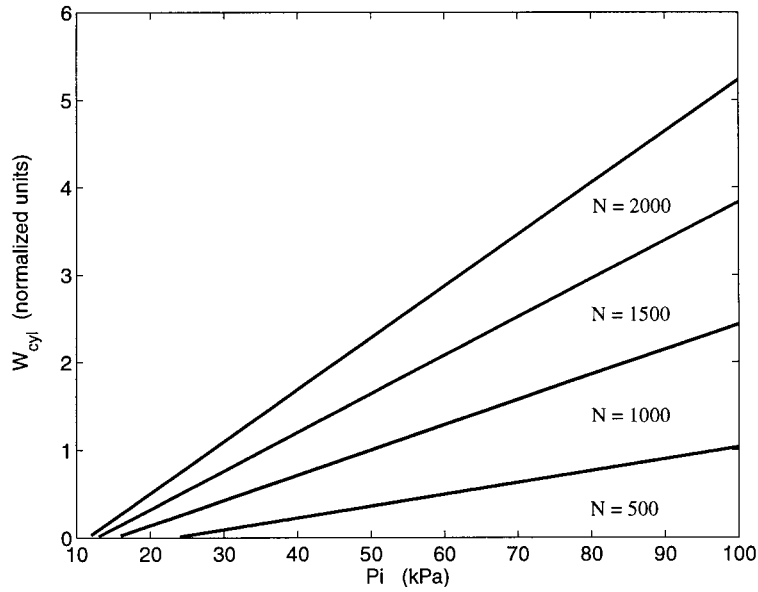
Figure 1. Representation of regressed W_{cyl} as a function of intake manifold pressure, P_i, (kPa) for various engine speeds, N (rpm). The plot has been scaled so that $W_{cyl} = 1$ at $N = 1000$ and $P_i = 50$.
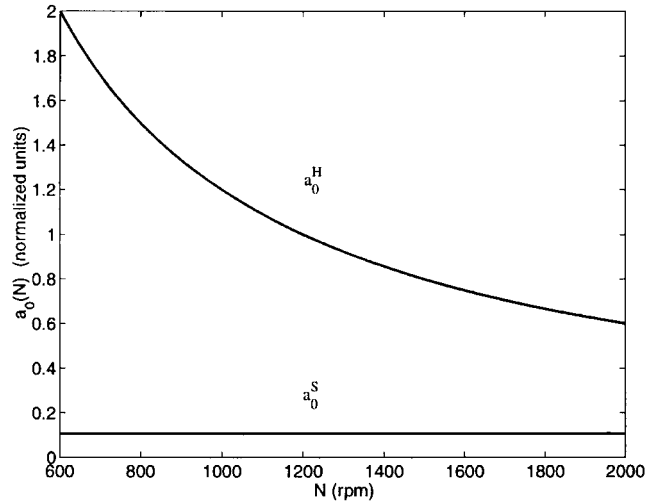

Figure 2. Representation of the regressed indicated torque functions, a_0^H and a_0^S, as a function of engine speed, N (rpm). The plot has been scaled so that $a_0^H = 1$ at $N = 1200$.

where

$$a = 0$$

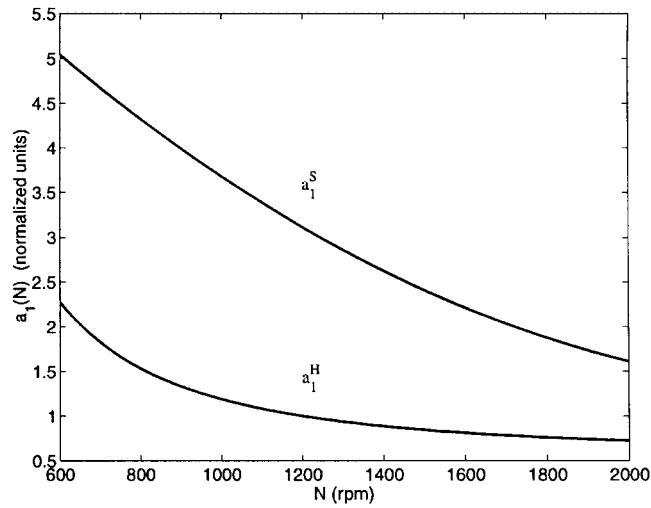$$b = \frac{A_{act}^{max} P_1}{\sqrt{T_1}} \phi(x)$$

Figure 3. Representation of the regressed indicated torque functions, a_1^H and a_1^S, as a function of engine speed, N (rpm). The plot has been scaled so that $a_1^H = 1$ at $N = 1200$.
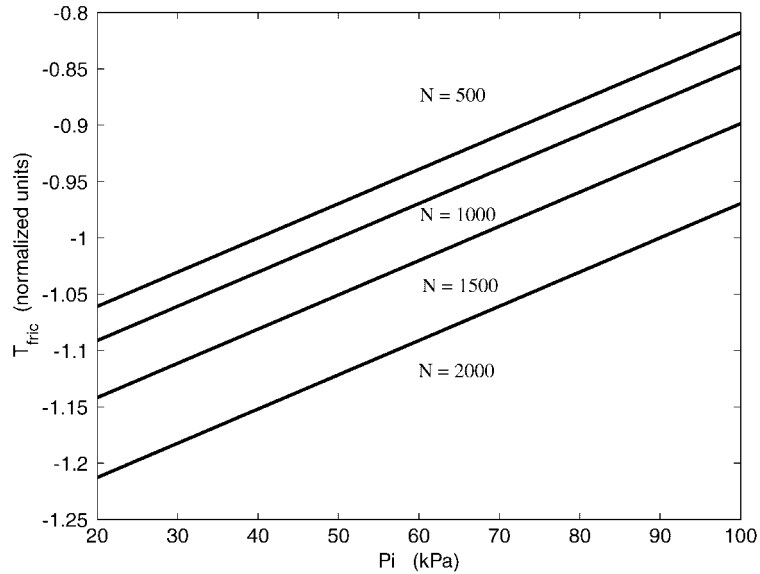

Figure 4. Representation of the regressed friction torque as a function of intake manifold pressure, P_i, (kPa) for various engine speeds, N (rpm). The plot has been scaled so that $\mathcal{T}_{\text{fric}} = -1$ at $N = 1000$ and $P_i = 50$.

$$P_1 = \begin{cases} P_{\text{amb}}, & \text{throttle} \\ P_{\text{e}}, & \text{EGR valve} \end{cases}$$

$$T_1 = \begin{cases} T_{\text{amb}}, & \text{throttle} \\ T_{\text{egr}}, & \text{EGR valve} \end{cases}$$

$$\phi(x) = \begin{cases} 4.04 \times 10^4 & \text{if } x \leqslant 0.53 \\ 1.56 \times 10^5 \sqrt{x^{1.4286} - x^{1.7143}} & \text{if } x > 0.53 \end{cases}$$

$$x = \frac{P_i}{P_1}$$

W_{act} (g/s) corresponds to the flow through the appropriate actuator, W_{th} or W_{egr}; W_{act}^{des} (g/s) is the desired mass flow rate through the actuator and A_{act}^{max} (m^2) is the effective flow area corresponding to a fully open valve. P_{amb} (kPa) and T_{amb} (K) correspond to the pressure and temperature at ambient conditions, respectively; P_e (kPa) is the exhaust manifold pressure and T_{egr} (K) is the temperature of the recirculated exhaust gas. Modelling errors will result in (3) being only approximately true. Such errors, however, should be well within the gain margins of any of the controllers proposed here. Moreover, the pre-compensators could be adapted on the basis of available measurements [19].

The air–fuel ratio in the cylinder is given by

$$r_c = \frac{(1 - F_i)W_{cyl}}{W_f} \tag{4}$$

In addition, the air–fuel ratio and burned gas fraction of the exhaust can be computed to be

$$r_e = \frac{F_i W_{cyl}(r_s/(r_s + 1)) + (1 - F_i)W_{cyl}}{F_i W_{cyl}(1/(r_s + 1)) + W_f} \tag{5}$$

$$F_e = \frac{r_s + 1}{r_e + 1} \tag{6}$$

where $r_s = 14.64$ is the stoichiometric air–fuel ratio. The expression for F_e and r_e are valid as long as $r_e \geqslant r_s$. When EGR is disabled, $F_i = 0$ and the expression for r_e is valid for all air–fuel ratios. These conditions are acceptable since, typically, no EGR is used when the engine is operated rich of stoichiometry.

2.2. Measurements

It is assumed that manifold pressure, P_i (kPa), engine speed, N (rpm), and exhaust air–fuel ratio, r_e, are measured and that the mass air-flow through the electronic throttle is not measured. Manifold pressure sensors have very high bandwidth [19, 20] and thus any sensor dynamics can be ignored.[||] A delay equal to one-third engine revolution, $d/3$, will be included to represent a reasonable sample rate. Engine speed is computed directly from crank shaft position and a delay of $d/3$ is also assumed. The exhaust air–fuel ratio is assumed to be measured with a linear sensor [21, 22] placed immediately after the exhaust manifold and before the emissions after-treatment system. The total delay from the induction event to the exhaust reaching the sensor is assumed to be $3d$. For simplicity, temperature-dependent aspects of the air–fuel ratio sensor are neglected and the sensor is assumed to function accurately, even in very lean conditions. The sensor's time constant is assumed to be 250 ms.

[||]Cylinder-to-cylinder pulsations are normally removed by averaging over one engine event.

In summary,

$$P_i^{\text{meas}}(t) = P_i\left(t - \frac{d}{3}\right)$$

$$N^{\text{meas}}(t) = N\left(t - \frac{d}{3}\right) \tag{7}$$

$$r_e^{\text{meas}}(t) = \frac{1}{0.25s + 1} r_e(t)$$

where

$$r_e(t) = \frac{F_i(t - 3d)W_{\text{cyl}}(t - 3d)(r_s/(r_s + 1)) + (1 - F_i(t - 3d))W_{\text{cyl}}(t - 3d)}{F_i(t - 3d)W_{\text{cyl}}(t - 3d)(1/(r_s + 1)) + W_f(t - 3d)}.$$

2.3. Cylinder mass-flow rate and burned gas fraction estimates

Since engine speed and manifold pressure are directly measured, the so-called 'speed-density' method [23] can be used to estimate cylinder mass flow rate:

$$\hat{W}_{\text{cyl}} = \alpha(N^{\text{meas}}) + \beta(N^{\text{meas}})P_i^{\text{meas}} \tag{8}$$

The burned gas fraction in the intake manifold is estimated via

$$\dot{\hat{m}}_{\text{bg}} = \hat{F}_e \hat{W}_{\text{egr}} - \hat{F}_i \hat{W}_{\text{cyl}}$$

$$\hat{F}_i = \frac{RT_i}{V} \frac{\hat{m}_{\text{bg}}}{P_i^{\text{meas}}} \tag{9}$$

where

$$\hat{F}_e = \frac{r_s + 1}{r_e^{\text{meas}} + 1}$$

$$\hat{W}_{\text{egr}} = \frac{A_{\text{egr}}\hat{P}_e}{\sqrt{\hat{T}_{\text{egr}}}} \phi\left(\frac{P_i^{\text{meas}}}{\hat{P}_e}\right) \tag{10}$$

Here, the exhaust manifold conditions are assumed constant with $\hat{P}_e = 105$ kPa and $\hat{T}_{\text{egr}} = 450$ K. In practice, more complex models of exhaust manifold pressure and EGR temperature may be necessary. It is also possible to implement estimation methods for burned gas fraction that do not require knowledge of exhaust conditions [19].

3. CONTROL OBJECTIVES AND CONTROLLER TOPOLOGY

The overall control objective is to idle the engine in the presence of load disturbances while maximizing fuel economy and minimizing tailpipe emissions. For a lean burn engine equipped

with a three-way catalyst (TWC) and a lean NO_x trap (LNT), this can result in the engine and emission system having four distinct operating policies:

P-1. If the engine and after-treatment system are sufficiently warmed-up, fuel economy is enhanced by operating the engine lean of stoichiometry. At low loads, stratified combustion can be used. Here, at loads typical for idle, a target air–fuel ratio of $30:1$ will be used.

P-2. At higher loads, stratified combustion may not be achievable due to air-flow constraints, but lean-homogeneous combustion may still be desirable. During lean operation, the TWC efficiently removes HC and CO from the engine's feedgas, and as long as the catalytic surfaces of the LNT are not saturated, the LNT will efficiently remove NO_x.

P-3. As the LNT's efficiency drops, its capacity must be regenerated by purging the trapped NO_x with reductants such as CO, HC and H_2 that are naturally produced during rich combustion. Here, a target air–fuel ratio of $14:1$ will be used for purging the LNT.

P-4. Finally, the engine could be operated at stoichiometry (nominally, an air–fuel ratio of $14.64:1$), where the TWC is designed to achieve an optimal trade-off in simultaneously removing HC, CO and NO_x from the engine's feedgas. This operating policy may be required, for example, when the temperature of the LNT is not within its efficient operating range.

For ease of implementation and on-vehicle calibration, SISO control strategies will be designed, rather than a multi-variable controller [24]. Hence, a single actuator must be associated with each low-level control objective. The choice of engine operating policy** determines how lower-level controllers should manage the overall control objectives of best fuel economy, lowest emissions and speed regulation in the presence of load disturbances. In P-1 and P-2, air–fuel ratio can be allowed to vary within a relatively wide range. Engine speed control can be given highest priority, and thus assigned to the fastest actuator, fuel. Air–fuel ratio is then regulated via the throttle to the set-point commanded by the supervisory controller to achieve best emission constrained fuel economy. In P-3 and P-4, air–fuel ratio must be held very near the commanded set-point, even at the expense of increased deviations in engine speed from its set-point. The faster actuator, fuel, is assigned to air–fuel ratio control and speed is regulated via the throttle.

This results in two distinct controller topologies, as shown in Figure 5, which will be termed the speed-dominant and the air–fuel ratio dominant topologies, respectively. As stated earlier, the supervisory controller will determine the desired combustion mode as part of the engine operating policy. In principle however, either controller topology could request that the supervisory controller command the engine to operate in either homogeneous or stratified combustion mode. Here the speed dominant topology is given authority to request a change in combustion mode during transients, if necessary to meet the highest priority objective of speed control. Thus the speed dominant topology is designed to operate in both combustion modes. When considering the air–fuel ratio-dominant topology, no deviation in combustion mode is allowed due to the strict requirement to maintain air–fuel ratio at the commanded set-point. Thus the air–fuel ratio dominant topology is designed to operate only in homogeneous combustion mode. The control system design will include individual SISO-controllers for these two topologies, as well as logic for mode transitions.

**As discussed in the Introduction, the choice of operating policy will be made by a supervisory controller, the design of which is not addressed in this paper.
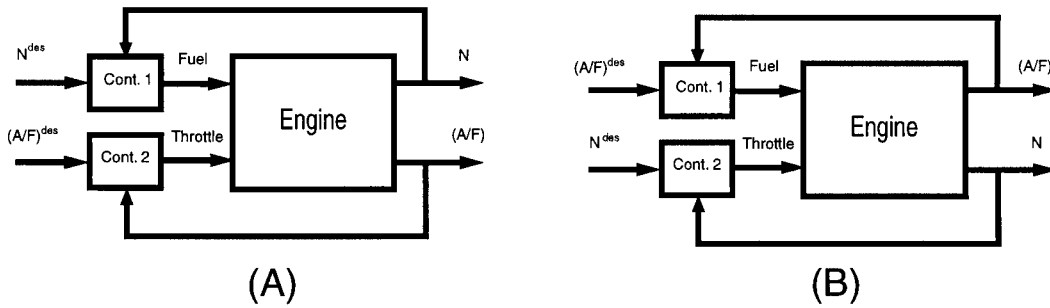
Figure 5. Controller Topologies: in (A), speed regulation is the dominant control objective, so it is associated with the faster actuator, fuel, while in (B), air–fuel ratio (A/F) regulation is the dominant control objective, so it is then associated with the faster actuator, fuel.

4. SPEED-DOMINANT CONTROLLER TOPOLOGY

This section considers idle speed control when fuel is selected as the primary actuator to affect torque. Here, air–fuel ratio is free to range from the rich limit of homogeneous combustion to the lean limit of stratified combustion and the combustion mode can vary between stratified and homogeneous as needed to meet the speed control objective. The control law development is based on Reference [25].

4.1. Initial speed control design

Suppose for the moment that brake torque, $\mathscr{T}_{b}(t) := \mathscr{T}_{i}(t) + \mathscr{T}_{fric}(t)$, can be directly controlled. Then the speed control problem amounts to designing a controller for the system

$$\dot{N}(t) = \frac{30}{\pi J_{e}} \left(\mathscr{T}_{b}(t-d) + \mathscr{T}_{fric}^{del}(t) - \mathscr{T}_{load}(t) \right)$$

$$N^{meas}(t) = N \left(t - \frac{d}{3} \right) \tag{11}$$

where $\mathscr{T}_{fric}^{del}(t) := (\mathscr{T}_{fric}(t) - \mathscr{T}_{fric}(t-d))$. The following assumptions are made to formulate a standard linear control problem:

- The term $\mathscr{T}_{fric}^{del}$ can be neglected. This term[††] will be small as long as the closed-loop system's bandwidth is less than $2/d$, which gives a bound of approximately 20 rad/s at idle conditions.
- Saturation issues will be addressed separately and are neglected for now.
- The load torque is unknown, but constant.
- The delays in (11) are represented by a first-order Padé approximation.

[††]This is *not* the same as neglecting $\mathscr{T}_{fric}$, though one could neglect friction and allow the integrator state of the controller (12) to account for it since friction essentially acts as a bias term.
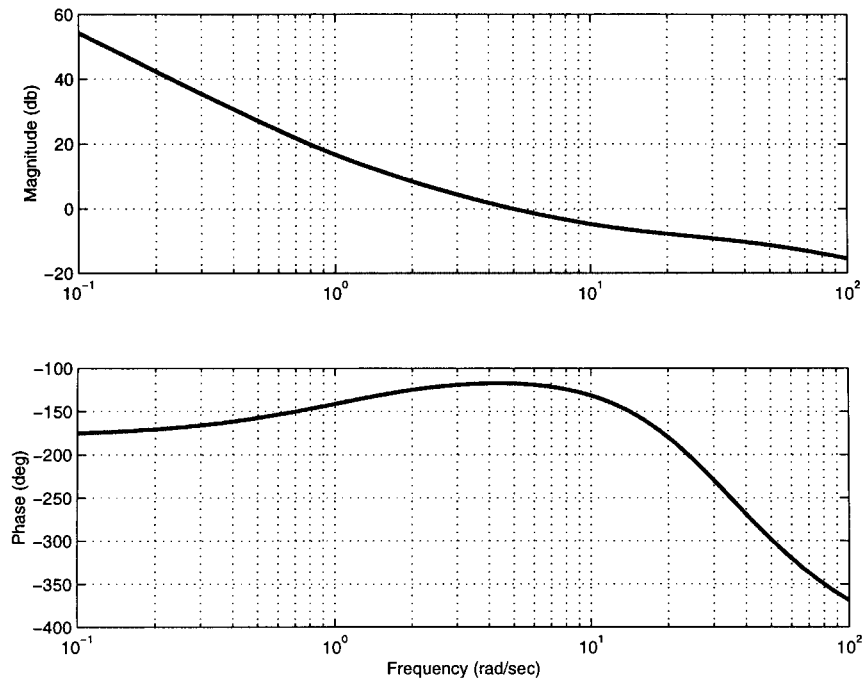
Figure 6. The Bode plot of (12) cascaded with (11).

In order to achieve zero steady-state error for constant engine speed commands, a PID-controller is appropriate. Using classical frequency domain design techniques results in the controller

$$\mathscr{T}_{b}(t) = C_0(s)(N^{\text{des}} - N^{\text{meas}})(t)$$

$$= \left(K_p + \frac{K_I}{s} + \frac{K_D s}{0.01s + 1} \right)(N^{\text{des}} - N^{\text{meas}})(t) \qquad (12)$$

where $K_P = 0.0727$, $K_I = 0.0750$ and $K_D = 0.0055$. Robustness to disturbances, plant uncertainty and measurement noise was addressed in this and all subsequent designs with careful attention to the sensitivity and complimentary sensitivity functions in the frequency range of interest.

The Bode plot of (12) cascaded with (11) is shown in Figure 6. The controller yields a gain cross-over frequency of 5 rad/s, a gain margin of 8 dB and a phase margin of 63°. The controller is valid for any speed–torque point of the engine's operation. The closed-loop bandwidth is limited by the time-delay, which is the sum of the measurement and combustion delays.[‡‡]

Of course, brake torque is not directly controllable. In order to obtain an implementable controller, the control signal (12) is first related to indicated torque via

$$\mathscr{T}_{i}^{\text{fuel}}(t) := C_0(s)(N^{\text{des}} - N^{\text{meas}})(t) - \widehat{\mathscr{T}}_{\text{fric}}(t) \qquad (13)$$

[‡‡]In a standard PFI engine with spark as the actuator, the time delay would be about half as much. Spark, however, has a limited range of actuation authority and can only be used as a secondary control actuator. The throttle must be the primary control actuator and as a result, the intake manifold dynamics introduce additional performance limitations.

and then to commanded fuel flow by the relationship for indicated torque

$$W_f(t) = \frac{T_i^{fuel}(t) - a_0(N^{meas}(t))(1 - \hat{F}_i(t))\hat{W}_{cyl}(t)}{a_1(N^{meas}(t))} \tag{14}$$

Here friction torque is estimated based on the model given in (2), using measurements of intake manifold pressure and engine speed. Compared to the standard fuel-based PID controller typically used for diesel applications [26], the advantage of the proposed algorithm is that it provides gain auto-scaling through the engine torque model via (13) and (14).

Since combustion mode is allowed to vary with this controller topology, a choice has to be made between homogeneous or stratified combustion, as this will determine the coefficients used in (14), $\{a_0^H, a_1^H\}$ or $\{a_0^S, a_1^S\}$. In this work, (14) a first solved assuming homogeneous combustion and the resulting in-cylinder air–fuel ratio, r_c, is estimated. If r_c is less than the lower bound on air–fuel ratio, in this case $12:1$, when W_f is recalculated such that r_c equals the lower bound and a request for homogeneous combustion is submitted to the supervisor. If r_c is within allowable bounds for homogeneous combustion, $12:1 \leqslant r_c \leqslant 19:1$, then homogeneous combustion is requested with no change to W_f. If r_c is too lean for homogeneous combustion, $r_c > 19:1$, then stratified combustion is requested,[§§] (14) is recomputed using $\{a_0^S, a_1^S\}$ and the resulting r_c is estimated. If necessary, W_f is saturated to enforce the upper or lower bound for r_c with stratified combustion, $19:1 \leqslant r_c \leqslant 40:1$.

The controller (14) can be applied as long as the air–fuel ratio stays within allowable bounds, such as $12:1$ to $40:1$. For the moment, this is assumed to be the case, and attention is now turned to how to control the electronic throttle and EGR valve in order to maintain desired set-points for air–fuel ratio and burned gas fraction. This will allow intermediate speed control simulations to be constructed. Then, the case of the fuel controller (14) resulting in saturation of W_f due to air–fuel ratio bounds, as discussed above, will be addressed.

4.2. Achieving EGR and air–fuel ratio set-points

As discussed in the Introduction, speed control must be integrated into a supervisory controller, which for given speed and load torque conditions, is charged with determining the optimal spark and fuel injection timings, burned gas fraction and air–fuel ratio settings for fuel economy and emissions [15]. Since the current speed control analysis assumes best spark and fuel injection timing, the remaining variables to be controlled are EGR and air–fuel ratio. Alternatively, intake manifold pressure or cylinder mass flow rate could be selected as the control variable instead of air–fuel ratio. Since fuel is being used to regulate engine speed, that leaves throttle as the actuator for air–fuel ratio.

4.2.1. Static aspects of EGR
The recirculated exhaust gas of a lean burn engine contains air as well as burned gas. For this reason, it is convenient to think of $W_{th} + W_{egr}$ as $W_{air} + W_{bg}$, where $W_{bg} = F_e W_{egr}$ is the mass flow rate of recirculated burned gas and $W_{air} = W_{th} + (1 - F_e)W_{egr}$ is the combined mass flow rate of

---

[§§]Although no chattering between modes was observed here, this could occur in practice. In this case, a form of hysteresis would be added to the switching logic. Also, a switch between modes normally requires a step change in fuel to achieve a given value of torque due to the different indicated torque maps associated with the homogeneous and stratified modes. This does not affect the dynamics of the controllers in any way.
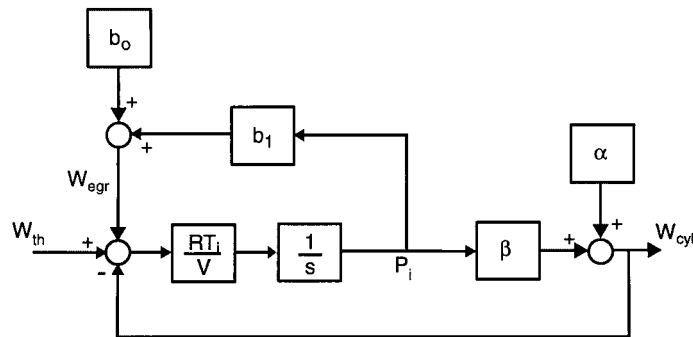
Figure 7. Block diagram of intake manifold system with EGR.

air from the throttle and recirculated exhaust gas. Once the EGR flow rate has been set, the electronic throttle command is then determined by $W_{th}^{des} = W_{air}^{des} - (1 - F_e)W_{egr}$, where W_{air}^{des} is the desired mass air flow rate. Of course, there will be inevitable inaccuracies in the estimation of W_{egr} and F_e, and hence in the determination of W_{th}^{des}. This must be compensated for by robustness of the control design.

EGR control is typically implemented in a feedforward (open-loop) manner, and this approach was followed here as well. The exhaust manifold was assumed to be nominally at 105 kPa and 450 K. Based on these nominal values, the method given in Reference [19] was used to maintain the intake manifold burned gas fraction at a desired level, such as $F_i = 0.1$.

4.2.2. Dynamic effects of EGR

At an air–fuel ratio of 30 : 1, achieving a burned gas fraction of 0.1 in the intake manifold requires more than twice as much recirculated exhaust gas as when the air–fuel ratio is at stoichiometry. Hence, a key element in understanding the system dynamics from throttle to cylinder mass flow is the effect of EGR on the intake manifold (or air charge) dynamics.

Linearizing the orifice flow equation for the EGR valve about a nominal operating point results in

$$W_{egr} \approx b_0(\text{steps}) + b_1(\text{steps})P_i \tag{15}$$

where steps represents EGR valve position, which is regulated by stepper motor. It is important to understand how the coefficients b_0 and b_1 vary with engine operating condition. The value of b_1 is of particular interest because it will directly affect the intake manifold dynamics. Assuming P_i is limited[¶] to 95 kPa, the minimum value of b_1 occurs when the valve is wide open, yielding $b_{1\min} = -0.16$. The maximum value occurs when the EGR valve is closed or flow is choked, yielding $b_{1\max} = 0$.

Given this representation of W_{egr} and the expression for W_{cyl} from (2), a block diagram of the intake manifold dynamics can be constructed and is illustrated in Figure 7. The plant model

[¶] EGR flow rate goes to zero as intake manifold pressure approaches exhaust manifold pressure. Since the orifice flow equation is not differentiable at $P_i = P_e$, linear analysis breaks down near this point.
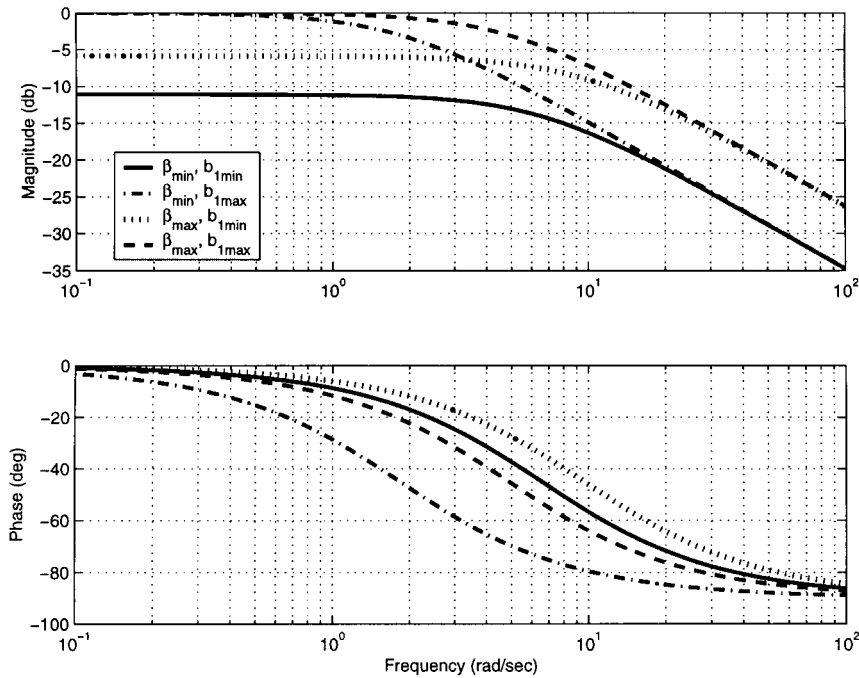
Figure 8. Bode plots of intake manifold system with model parameter variations due to EGR.

needed for control development is given by the transfer function from W_{th} to W_{cyl}. Considering only small signal analysis and thus neglecting the influence of α and b_0, define

$$K_V := \frac{R T_i}{V}$$

then

$$W_{cyl}(s) = \frac{K_V \beta}{s + K_V(\beta - b_1)} W_{th}(s) \qquad (16)$$

Thus the model parameters b_1 and β directly affect the DC-gain and the pole. This is illustrated with Bode plots of (16), shown in Figure 8. Plots are shown for each combination of minimum and maximum parameter values. Therefore, the controllers developed to actuate the throttle must be robust to at least this amount of model uncertainty.

4.2.3. Air–fuel ratio control
Assuming that exhaust air–fuel ratio can be measured accurately under very lean conditions, (5) can be used to obtain an estimate of the flow rate into the cylinder by

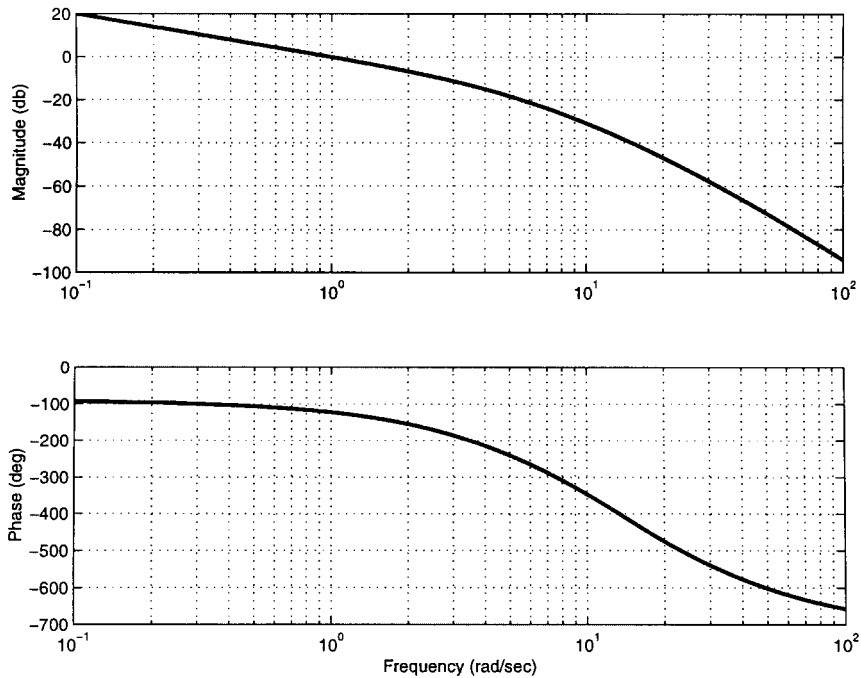$$\hat{W}_{cyl}(t) = \frac{W_f(t - 3d)}{1 - \hat{F}_i(t)(r_e^{meas}(t) + 1)/(r_s + 1)} r_e^{meas}(t) \qquad (17)$$

Figure 9. Bode plots for the cascade of the controller (20) with the system (18).

This can be used to replace the air–fuel ratio control problem with one of designing a set-point controller for the system

$$\dot{P}_i = \frac{RT_i}{V}(W_{th} + W_{egr} - W_{cyl})$$

$$y = (1 - F_i)W_{cyl}(t - 3d) \tag{18}$$

Classical design rules lead to the PI controller

$$W_{th}(t) = \left(K_P^1 + \frac{K_I^1}{s}\right)(y^{des}(t) - y(t)) \tag{19}$$

with $K_P^1 = 0.45$, $K_I^1 = 1$ and y^{des} equal to (17) with r_e^{meas} substituted by r_e^{des}. The associated Bode loop gain is shown in Figure 9. The controller (19) was slightly simplified and implemented on the DISC engine as

$$W_{th}(t) = \left(K_P^1 + \frac{K_I^1}{s}\right)\left(\frac{1}{1 - \hat{F}_i(t)(r_e^{meas}(t) + 1)/(r_s + 1)}\right)W_f(t - 3d)(r_e^{des}(t) - r_e^{meas}(t)) \tag{20}$$

Remark

An advantage of working with (17) instead of $(r_e^{des} - r_e^{meas})(t)$ alone is that the term

$$\frac{W_f(t - 3d)}{1 - \hat{F}_i(t)(r_e^{meas}(t) + 1)/(r_s + 1)} \tag{21}$$
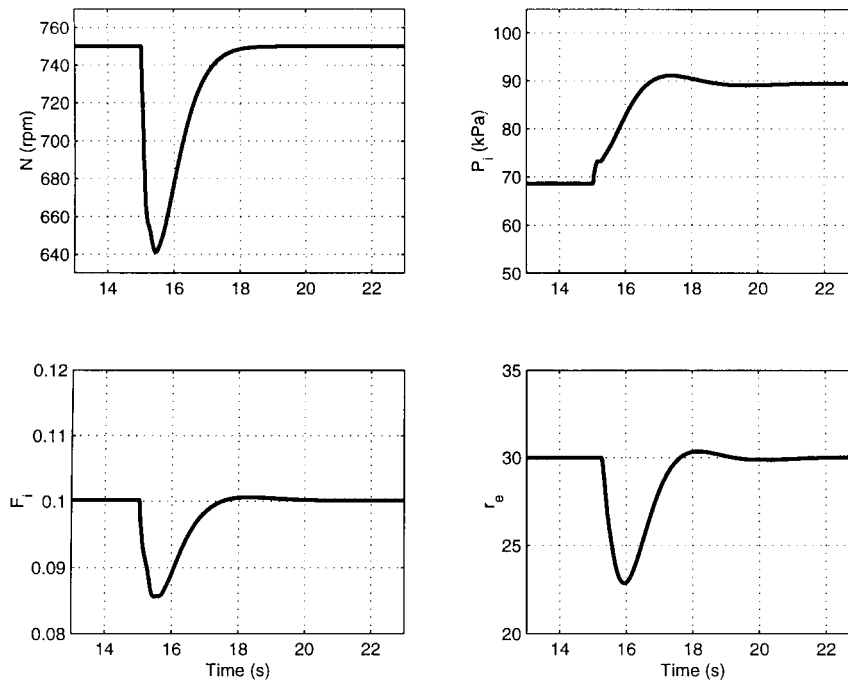
Figure 10. Torque step from 10 to 20 Nm applied at time 15 s. EGR set-point of $F_i = 0.1$ and air–fuel ratio set-point of $30:1$.

includes W_f, which automatically schedules the controller gains as a function of engine operating points. If one did not wish to rely on measured r_e, control could be done on the basis of estimated in-cylinder air–fuel ratio instead of measured exhaust air–fuel ratio.

Due to the long time delay in the air–fuel ratio loop, the controller (20) will respond slowly to a change in commanded set-point. During a commanded purge however, fuel economy is enhanced by making the transition to a rich air–fuel ratio as quickly as possible. For this reason, during a commanded transition from lean to rich operation, (20) is replaced with[||]

$$W_{th}(t) = \frac{W_f(t)}{1 - \hat{F}_i(t)} r_e^{des} \tag{22}$$

4.3. Intermediate simulations

Figure 10 shows the response of the closed-loop system to a step in engine load torque*** from 10 to 20 Nm at time 15 s. It is seen that without any feedforward information on the load step, the

---

[||]Switching from (20) to (22) provides a faster response than using a feedforward plus feedback configuration. The method used for switching is explained in Section 6.
***This common form of disturbance is typically introduced by accessory loads. Possible accessories include air conditioner, alternator, power steering, etc.
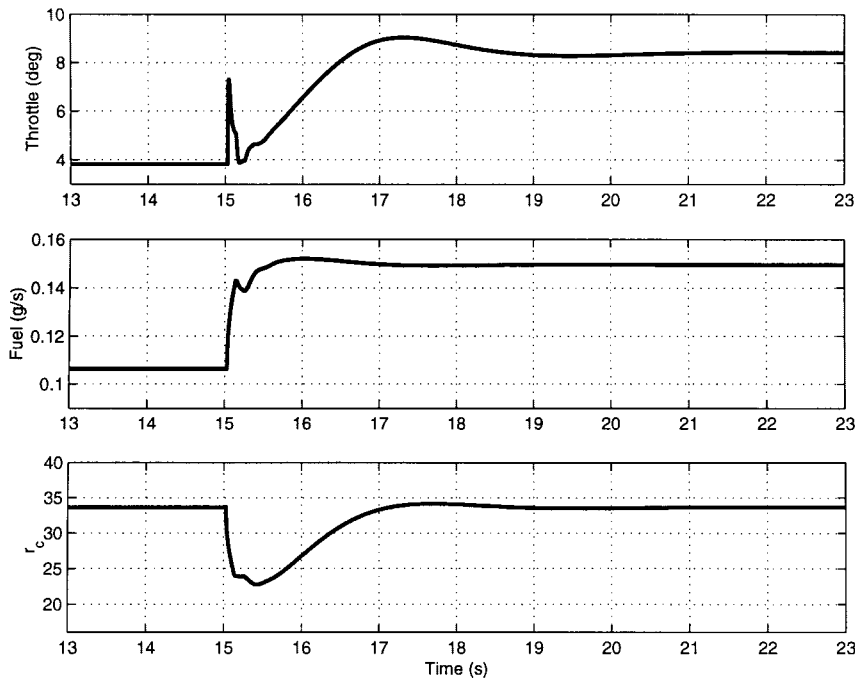
Figure 11. Actuators and in-cylinder air–fuel ratio for torque step from 10 to 20 Nm applied at time 15 s. EGR set-point of $F_i = 0.1$ and air–fuel ratio set-point of 30:1.

speed droops by approximately 108 rpm from the assumed set-point of 750 rpm. Rapid torque response[†††] is obtained by decreasing the air–fuel ratio to 23:1 from the desired set-point value of 30:1. The throttle to air–fuel ratio controller then moves the air–fuel ratio back to the assumed optimal position. This was possible because the load was sufficiently small that the commanded air–fuel ratio could be achieved without actuator, air–fuel ratio or manifold pressure saturation. The associated actuator responses are shown in Figure 11. Due to space constraints, these will not be displayed for other operating conditions.

4.4. Addressing air–fuel ratio bounds

In response to a sufficiently large added load torque, the controller (14) will command a value of fuel that will result in an air–fuel ratio that exceeds a desired lower bound, R_1, say 12:1. Also, in response to the removal of a sufficiently large load, it will command a value of fuel resulting in an air–fuel ratio that is higher than an allowable upper bound, R_2, say the lean limit. In either case, the fuel flow rate is effectively saturated. Since speed control is of higher priority than air–fuel

---

[†††]Note that at 750 rpm, the combined combustion and measurement delay is approximately 0.11 s, and thus with an engine inertia of 0.141 (Nm s²), a 10 Nm load increase and will result in a speed drop of approximately 73 rpm before the engine torque can possibly respond.
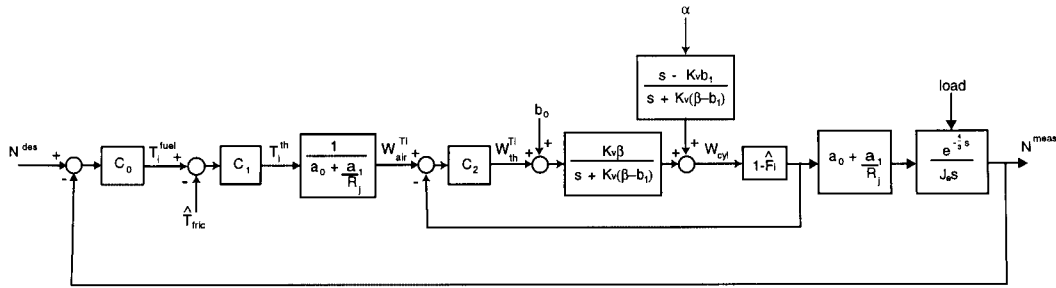
Figure 12. Speed controller architecture when fuel is saturated and throttle is the primary actuator.

ratio set-point optimality, the throttle must be re-assigned for speed control. This subsection develops a throttle controller to be used for speed regulation when the fuel saturates.

Let $[R_1, R_2]$ be the allowed range of air–fuel ratios. Assume that W_f has been limited to meet the air–fuel ratio bounds, so that $W_f = (1 - F_i) W_{cyl}/R_j$, where

$$R_j = \begin{cases} R_1 & \text{when air–fuel ratio equals the rich limit} \\ R_2 & \text{when air–fuel ratio equals the lean limit} \end{cases} \tag{23}$$

Then torque is determined by air flow. On this basis, the indicated torque can be re-written as

$$\mathcal{T}_i = (a_0(N) + a_1(N)/R_j)(1 - F_i) W_{cyl} \tag{24}$$

and solved for W_{cyl} in order to obtain the desired mass flow rate out of the intake manifold as a function of desired indicated torque. The question at hand can be viewed as one of determining a proper controller for the throttle so that this is achieved.

Figure 12 depicts the controller architecture employed for regulating speed via the throttle when fuel is saturated based on air–fuel ratio constraints. The structure of the controller is highly suggestive of an inner–outer loop design from classical control. This structure allows throttle-based speed control to be integrated with the fuel-based speed controller, (12)–(14), with considerable ease, as will be seen.

Linear time-invariant compensators $C_1(s)$ and $C_2(s)$ were designed on the basis of classical frequency domain design rules. Figure 13 displays the loop gain from speed error, $N^{des} - N^{meas}$, to N^{meas} for the compensators

$$C_1(s) = \frac{(1.32s + 1)}{0.01s + 1} \tag{25}$$

$$C_2(s) = 0.115 \tag{26}$$

for the extremes of model variation due to EGR. The controller design is robust to the inclusion of EGR and results in a minimum gain margin of 11 dB and phase margin of $46°$ when EGR is varied as in Figure 7. The DC gain of the load term, $C_1(s)$, has been deliberately set to 1.0 and the overall loop gain adjusted with $C_2(s)$. The purpose of the lead term is to compensate for the phase lag due to the intake manifold filling dynamics. The output of the fuel-based speed controller can be passed through the lead term $C_1(s)$ in order to compute the commanded indicated torque for
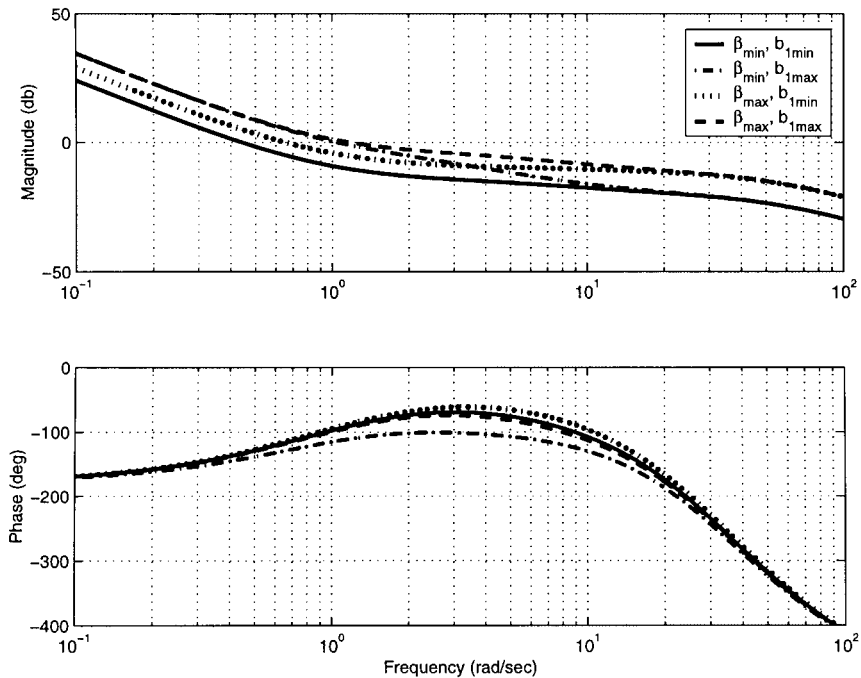
Figure 13. Bode plots for the throttle based speed control cascaded with the engine model for the extremes of model variations due to EGR.

the throttle-based speed controller,

$$\mathcal{T}_{\mathrm{i}}^{\mathrm{th}}(t) := C_1(s)(C_0(s)(N^{\mathrm{des}} - N)(t) - \hat{\mathcal{T}}_{\mathrm{fric}}(t)) \tag{27}$$

From this, it is clear that only the integrator in $C_0(s)$ will have to be protected by anti-windup logic.

The speed-throttle controller should only be active when the speed-fuel controller results in effective saturation of the fuel. The control architecture has been designed to enforce this requirement. To see this, define

$$\hat{r}_{\mathrm{c}}(t) := \frac{(1 - \hat{F}_{\mathrm{i}}(t))\hat{W}_{\mathrm{cyl}}(t)}{W_{\mathrm{f}}(t)} \tag{28}$$

which is the current (estimated) in-cylinder air–fuel ratio. Also, define

$$R(t) := \begin{cases} R_1 & \hat{r}_{\mathrm{c}}(t) \leqslant R_1 \\ \hat{r}_{\mathrm{c}}(t) & R_1 < \hat{r}_{\mathrm{c}}(t) < R_2 \\ R_2 & \hat{r}_{\mathrm{c}}(t) \geqslant R_2 \end{cases} \tag{29}$$

and

$$W_{\mathrm{air}}^{\mathcal{T}_{\mathrm{i}}} = \frac{\mathcal{T}_{\mathrm{i}}^{\mathrm{th}}}{a_0 + a_1/R} \tag{30}$$
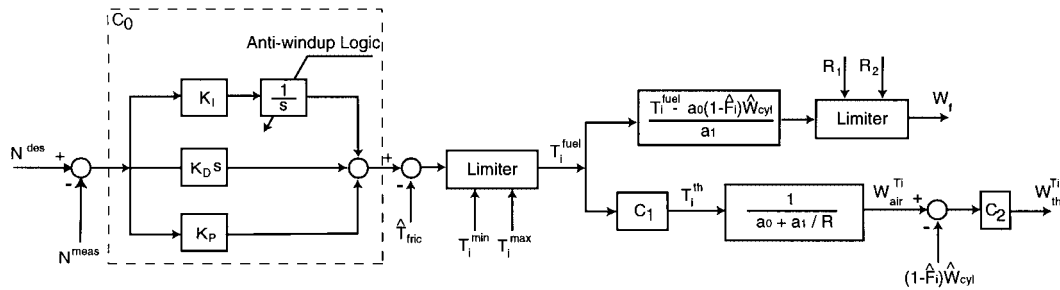
Figure 14. Schematic representation of the modifications to the basic speed controller.

Then by construction, since $C_1(s)$ is BIBO stable and has unity DC-gain, if $R(t) = \hat{r}_c(t)$,

$$\lim_{t \to \infty} (W_{\mathrm{air}}^{\mathscr{T}_i} - (1 - \hat{F}_i)\hat{W}_{\mathrm{cyl}})(t) = 0 \tag{31}$$

under steady-state conditions (recall that, by design, $C_1(s)$ has a DC-gain of unity). Thus

$$W_{\mathrm{th}}^{\mathscr{T}_i} = C_2(s)(W_{\mathrm{air}}^{\mathscr{T}_i} - (1 - \hat{F}_i)\hat{W}_{\mathrm{cyl}}) \tag{32}$$

will be asymptotically zero when the estimated in-cylinder air–fuel ratio is strictly within the allowable bounds given by R_1 and R_2, and will implement the speed-throttle controller otherwise.

4.5. Additional nonlinearities and logic to deal with saturation

Several more issues must be addressed before the compensators (12), (20), (25) and (26) can be integrated into a functional speed controller. Each issue is a direct or indirect consequence of saturation.

Issue-1. The engine produces limited indicated torque, whereas (12) and (25) implicitly assume that $\mathscr{T}_i$ is not bounded from above or below. When the engine is producing its maximum or minimum torque, anti-windup logic must be placed around the integrator in (12).

Issue-2. The overall speed controller must deal with at least two modes of operation. In the first mode, both fuel and throttle are unsaturated, and consequently, both speed and optimal set-point objectives can be pursued by the controller. In this mode, it is still possible that the planned set-point cannot be achieved due to the manifold pressure reaching its maximum. Anti-windup logic is thus necessary around the integrator of (20). In the second mode, fuel is saturated, and only the speed objective can be pursued. The transition between these two modes must be addressed. This includes when to activate the integrator in (20) and when to deactivate it.

Issue-3. Since indicated torque is non-negative, the removal of a large load can result in significant speed 'flare', followed by speed undershoot, unless a 'dashpot' type of action is incorporated into the controller.

The modifications to the basic controller are illustrated in Figure 14. Details of the implementations, although non-trivial, are straightforward and are only briefly summarized here. To deal with Issue-1, the integrator on the speed error in (12) is deactivated when the commanded
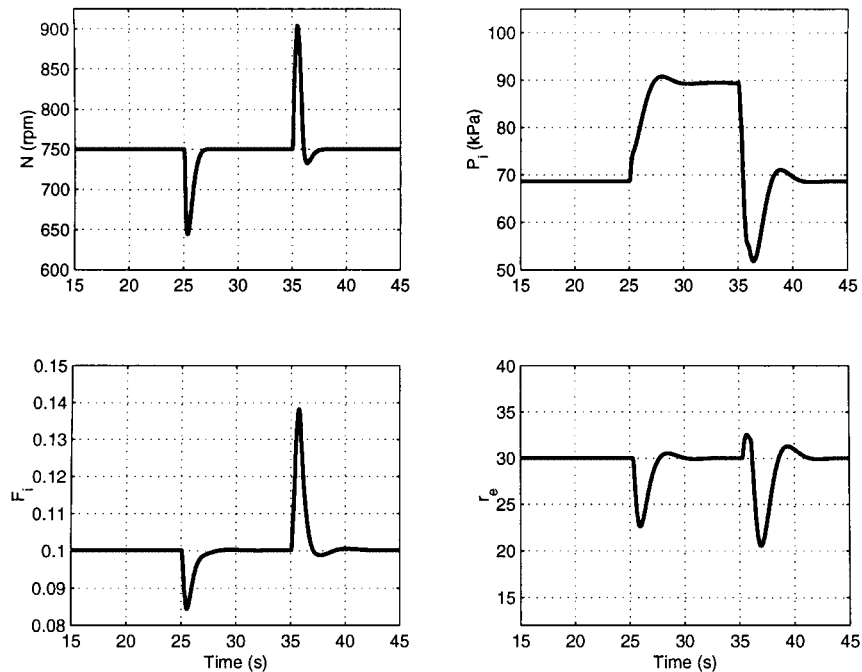
Figure 15. Torque step from 10 to 20 Nm applied at time 25 s and back to 10 Nm at 35 s. EGR set-point of $F_i = 0.1$ and air–fuel ratio set-point of 30:1.

indicated torque exceeds upper or lower bounds to prevent wind-up associated with the fuel actuator. In Issue-2, the integrator on air–fuel error in (20) is deactivated when either manifold pressure or throttle position exceed upper or lower bounds to prevent wind-up associated with the throttle. To address Issue-3, during tip-out, the integrator in (20) is commanded to achieve a manifold pressure set-point, the value of which is selected on the basis of estimated load torque. The goal is to initially reduce manifold pressure in order to provide significant friction torque for engine braking, and then to recenter the manifold pressure at a point where the fuel controller is unsaturated and hence capable of controlling the engine to achieve the speed set-point.

4.6. Illustrative simulations

Figure 15 depicts the concerted action of the controllers (12), (20), (25) and (26) when the load torque is stepped from 10 to 20 Nm at time 25 s and back to 10 Nm at 35 s; the EGR set-point is $F_i = 0.1$ and the exhaust air–fuel ratio set-point is 30:1. The sudden removal of the load results in a speed flare of 150 rpm. The controller uses rapid engine braking to bring the speed back to within 2 per cent of the nominal 750 rpm set-point in less than 1 s. Figure 16 illustrates a similar situation except the load is stepped from 20 to 30 Nm and back to 20 Nm. Note that at a 30 Nm load, the throttle is effectively saturated since the intake manifold pressure has been limited to 95 kPa. Consequently, the system cannot achieve the exhaust air–fuel ratio set-point of 30:1 with $F_i = 0.1$.
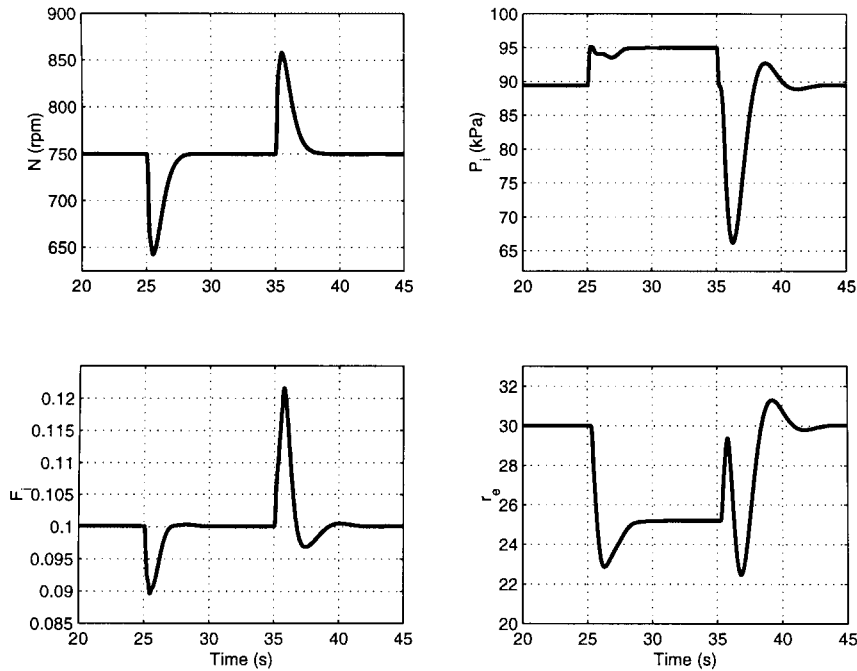
Figure 16. Torque step from 20 to 30 Nm applied at time 25 s and back to 20 Nm at 35 s. EGR set-point of $F_i = 0.1$ and air–fuel ratio set-point of 30:1.

5. AIR–FUEL RATIO-DOMINANT CONTROLLER TOPOLOGY

The control topology most commonly associated with idle speed control for stoichiometric engines has fuel assigned to air–fuel ratio regulation and throttle, possibly assisted by spark timing, assigned to speed regulation. EGR is typically disabled to maintain stable homogeneous combustion at idle conditions. The control law development for this topology is standard [10, 14]; consequently, the development will be brief.

5.1. Air–fuel ratio control

Air–fuel ratio control is accomplished with a combination of feedforward and feedback control of fuel [10, 14]. The feedforward term is given by dividing the estimated cylinder air flow by the commanded in-cylinder air–fuel ratio. The feedback term is a PI-controller applied to the exhaust air–fuel ratio error. Thus,

$$W_f(t) = \frac{\hat{W}_{cyl}(t)(1 - \hat{F}_i(t))}{r_c^{des}} + \left(K_p + \frac{K_i}{s}\right)(r_e^{des} - r_e^{meas}(t)) \tag{33}$$

The controller gains are determined by linearizing the model about a nominal speed of 750 rpm, 10 Nm load, no EGR and stoichiometric air–fuel ratio, and applying classical design

techniques. This results in the gains $K_p = -0.004$ and $K_i = -0.0087$, which yield a bandwidth of approximately 1.7 rad, a gain margin of 15 dB and a phase margin of $85°$. The bandwidth of the feedback loop is limited by the large time delay in the air–fuel ratio path.

5.2. Speed control

Speed control is accomplished with feedback control of mass air flow through the electronic throttle.[‡‡‡] Control law development for this topology is well documented in the literature [10, 14]. The first step is to linearize the model about a nominal speed, load, and air–fuel ratio, with no EGR. This yields the transfer function

$$\frac{N(s)}{W_{th}(s)} = \frac{1}{sV/RT_i\beta(N^{des}) + 1}\left(a_0(N^{des}) + \frac{a_1(N^{des})}{r_c^{des}}\right)(1 - F_i)\frac{30}{\pi J_e s}e^{-4/3\,ds} \tag{34}$$

A PI plus lead compensator acting on the speed error would then be designed.

Here, in view of aiding the transition process between the speed-dominant and air–fuel ratio-dominant control topologies, the above approach will be slightly modified. Similar to the approach taken with the speed-dominant topology, assume that torque, T_i^{th}, can be directly controlled, resulting in the transfer function

$$\frac{N(s)}{T_i^{th}(s)} = \left(\frac{1}{Vs/RT_i\beta(N^{des}) + 1}\right)(1 - F_i)\frac{30}{\pi J_e s}e^{-4/3\,ds} \tag{35}$$

Classical techniques were used to design the controller

$$C_{PID,lead}(s)(N^{des} - N^{meas}(t)) = C_0(s)C_3(s)(N^{des} - N^{meas}(t)) \tag{36}$$

where C_0 was designed in Section 4 and C_3 is given by

$$C_3(s) = 0.25\frac{(s + 1.95)}{0.01s + 1} \tag{37}$$

The resulting minimum gain and phase margins are 6.6 dB and $55°$, respectively, even if EGR were to be used. The controller can then be implemented on the DISC engine via

$$W_{th}(t) = \frac{1}{a_0(N^{des}) + a_1(N^{des})/r_c^{des}}C_{PID,lead}(s)(N^{des} - N^{meas}(t)) \tag{38}$$

or, by solving the indicated torque equation, via

$$W_{th}(t) = (C_{PID,lead}(s)(N^{des} - N^{meas}(t)) - a_1(N^{des})W_f(t))\frac{1}{a_0(N^{des})} \tag{39}$$

The latter formulation, which is similar to the speed control methodology of Section 4.1, is used here.

[‡‡‡]On an engine equipped with a standard manual throttle, the air flow would be varied by the air by-pass valve, which is a type of electronic throttle in parallel with the manual throttle valve.
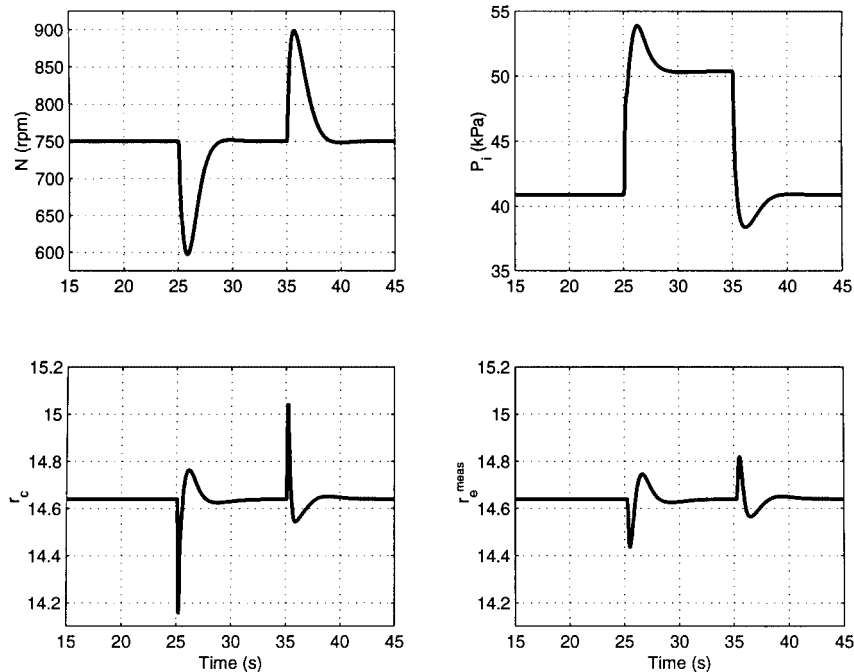
Figure 17. Torque step from 10 to 20 Nm applied at time 25 s and back to 10 Nm at 35 s. EGR set-point of $F_i = 0.0$ and air–fuel ratio set-point of 14.64 : 1 (stoichiometry).

5.3. Intermediate simulation

Figure 17 is analogous to Figure 15, except here the air–fuel ratio-dominant topology is used. The nominal set-points are 750 rpm, stoichiometric air–fuel ratio and no EGR. The load torque is stepped from 10 to 20 Nm at time 25 s, resulting in a speed droop of 153 rpm, and then back to 10 Nm at 35 s, resulting in a speed flare of 150 rpm. The corresponding values for the speed-dominant controller topology were 109 and 150 rpm, respectively. The maximum measured exhaust air–fuel ratio deviation is 0.19 while the modelled in-cylinder air–fuel ratio deviation is 0.4.

6. PUTTING IT ALL TOGETHER

The engine model and controller are implemented in MATLAB/Simulink®. MATLAB and Simulink are registered trademarks of the Mathswork, Inc. An elementary supervisor is employed to decide the set-points for engine idle speed, air–fuel ratio and intake burned gas fraction. The supervisor's default objective is to idle at 750 rpm, with an exhaust air–fuel ratio of 30 : 1 and $F_i = 0.1$, resulting in the use of the speed-dominant control topology. After a period of lean-idle,
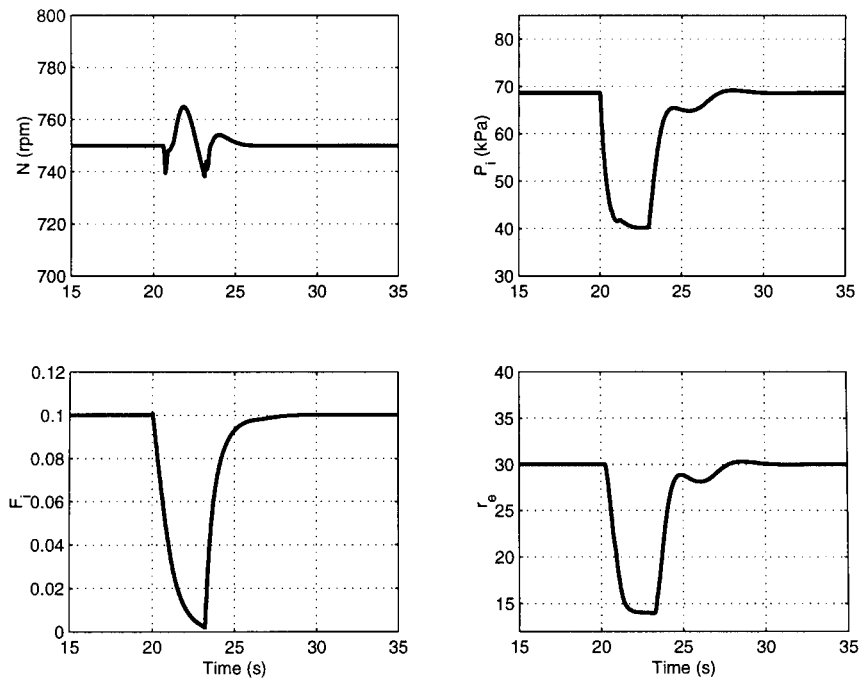
Figure 18. Purge of the LNT. EGR set-point of $F_i = 0.1$ and nominal air–fuel ratio set-point of $30:1$. In-cylinder air–fuel ratio achieved $14:1$ in 1 s.

the supervisor must purge the NO_x trap. The objective then is to transition rapidly to an air–fuel ratio[§§§] of $14:1$ and $F_i = 0.0$. This is accomplished with a step change of the air–fuel ratio and burned gas fraction set-points[¶¶¶] to $13.5:1$ and 0.0, respectively. Initially, the idle speed control maintains the speed-dominant topology in stratified mode. The speed-dominant topology requests a change to homogeneous combustion mode when the in-cylinder air–fuel ratio becomes less than or equal to $19:1$ and F_i is small. When the estimated in-cylinder air–fuel ratio attains $14:1$, the supervisor transitions to the air–fuel ratio-dominant topology with set-points 750 rpm, $14:1$ and 0.0. This topology is necessary because optimal purging requires that the air–fuel ratio set-point be accurately maintained, even during a load disturbance. After two seconds of rich idle, the NO_x purge is terminated. The supervisor returns the idle speed controller to the speed-dominant control topology, which initially requests homogeneous combustion. The set-point for exhaust air–fuel ratio is stepped up to $25:1$, held for 1 s, and then ramped up to $30:1$ at a rate of 2 air–fuel ratios per second at the direction of the supervisor. Once conditions suitable for stratified combustion are achieved, r_c greater than $19:1$, the commanded burned gas fraction is stepped up to 0.1 and a request for stratified combustion is issued.

[§§§]With no EGR, the in-cylinder and exhaust air–fuel ratios are identical in steady state.
[¶¶¶]Since air–fuel ratio will asymptotically approach the set-point, an air–fuel ratio of $13.5:1$ is commanded to assure that an air–fuel ratio crossing will occur at $14:1$ in a small, finite amount of time.
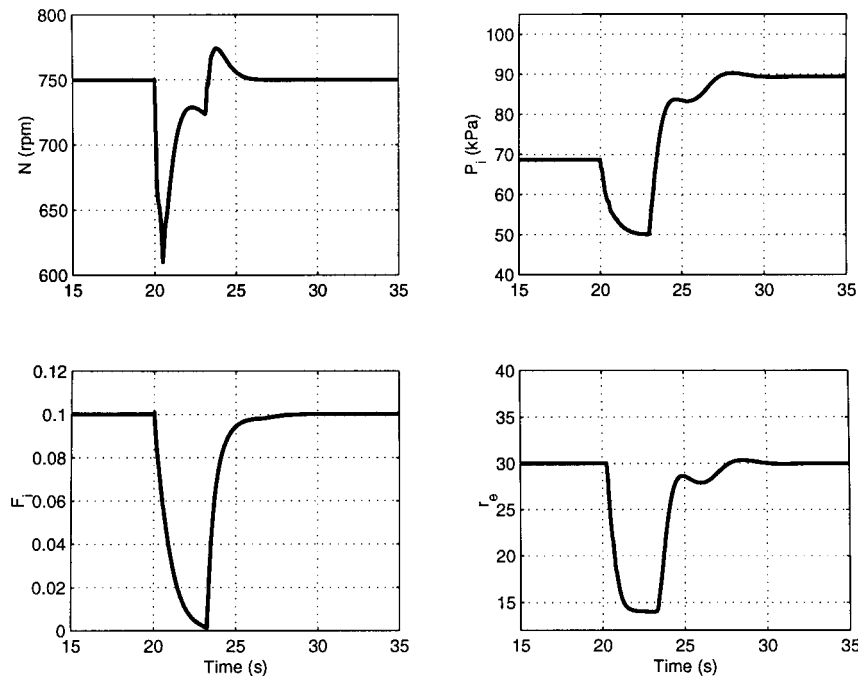
Figure 19. Step load change from 10 to 20 Nm at time 20 s, the beginning of the purge of the LNT. EGR set-point of $F_i = 0.1$ and nominal air–fuel ratio set-point of 30:1.

In order to assure a bumpless transfer between the two controller topologies and to stabilize the controller that is not switched into the closed-loop, the method of Reference [27, p. 566] was used. This choice was made on the basis of its ease of implementation in MATLAB/Simulink®. In practice, the controller not in the loop may not be executed; when switched into the loop, its state would then be re-initialized to minimize jumps in the actuator values or commanded indicated torque.

Figure 18 shows the results of initiating a purge at time 20 s under a nominal constant load of 10 Nm, EGR set-point of $F_i = 0.1$ and exhaust air–fuel ratio set-point of 30:1. The transition from an in-cylinder air–fuel ratio of 34:1 to rich of stoichiometry is accomplished in 0.9 s. The air–fuel ratio is held at 14:1 for 2 s, and then transitioned back to the nominal set-point. The transition from an in-cylinder air–fuel ratio of 14:1 to greater than 30:1 is accomplished in approximately 1 s.|||| While the air–fuel ratio is making these transitions, the maximum speed deviation is 15 rpm. Figure 19 shows a similar situation with the exception that a step change in load from 10 to 20 Nm occurs at time 20 s, which coincides with the beginning of the purge of the LNT. The EGR and nominal air–fuel ratio set-points are as before. The maximum deviation in speed is 140 rpm, which lies between the maximum speed deviation resulting from a 10 Nm load

||||The increase in engine-out emissions that may result from air–fuel ratios transients during mode transitions are effectively handled by the after-treatment system.

disturbance in the speed-dominant and air–fuel ratio-dominant topologies when a purge is not taking place. In terms of the key parameters for the purging process, the air–fuel ratio and EGR responses are virtually identical to the case of no load disturbance.

7. CONCLUSION AND SUGGESTIONS FOR FUTURE WORK

This paper has developed an idle speed controller for a DISC engine. For implementation reasons, individual subsystem controllers were based on SISO design methodology. Two controller topologies were needed in order to fully exploit the multiple combustions modes (stratified and homogeneous) and objectives (lean idle, stoichiometry and purge) of the engine. When integrated together with a supervisor, the controllers were able to make the transition from lean idle to purge in less than 1 s, and back to lean idle in a few seconds, while rejecting a load disturbance of ± 10 Nm with a maximum engine speed deviation of 155 rpm.

In developing the controller, a number of simplifying assumptions have been made. It would be interesting to develop a control design that exploited the reduced fuel injection time delay in the stratified mode. In particular, when a decision to use stratified combustion has been made at one revolution prior to spark ignition, the amount of fuel to be injected could be re-computed at one half revolution prior to spark ignition, reducing the delay to $d/2$. It would also be very interesting to understand how much the overall performance of the controller could be improved through a fully MIMO design methodology [24]. This would primarily benefit the stratified combustion mode.

REFERENCES

1. Elrod AC, Nelson MT. Development of a variable valve timing engine to eliminate the pumping losses associated with throttled operation. *SAE Paper* (860537), 1986.
2. Leone TG, Christenson EJ, Stein RA. Comparison of variable camshaft timing strategies at part load. *SAE Paper* (960584), 1996.
3. Vogel O, Roussopoulos K, Guzzella L, Czekaj J. Variable valve timing implemented with a secondary valve on a four cylinder SI engine. *1997 Variable Valve Actuation and Power Boost SAE Special Publications,* 1258(970335), February 1997; 51–60.
4. Ashhab MS, Stefanopoulou AG, Cook JA, Levin M. Camless engine control for robust unthrottled operation. *SAE Paper* (981031), 1998.
5. Kang J, Grizzle JW. Nonlinear control for joint air and fuel management in a SI engine. *Proceedings of the American Control Conference*, San Diego, 1999.
6. Heywood JB. *Internal Combustion Engine.* McGraw-Hill: New York, 1988.
7. Brogan, MS, Brisley RJ, Walker AP, Webster DE, Boegner W, Fekete NP, Krämer M, Krutzsch B, Voigtländer D. Evaluation of NO_x storage catalyst as an effective system for NO_x removal from the exhaust gas of lean-burn gasoline engines. *SAE Paper* (952490), 1995.

8. Fekete N, Kemmler R, Voigtländer D, Krutzsch B, Zimmer E, Weinninger G, Strehlau W, van den Tillaart JAA, Leyrer J, Lox ES, Müller W. Evaluation of NO_x storage catalyst for lean burn gasoline fueled passenger cars. *SAE Paper* (970746), 1997.

9. Wang Y, Raman S, Grizzle JW. Lean NO_x trap modeling for lean burn engine control. *1999 American Control Conference*, June 1999.

10. Cook JA, Grizzle JW, Sun J. *Engine Control*. Electrical Engineering Handbook Series. CRC Press: Boca Raton, FL, 1995.

11. Hrovat D, Sun J. Models and control methodologies for ic engine idle speed control design. *Control Engineering Practice* 1997; **5**(8):1093–1100.

12. Yurkovich S, Simpson M. Comparative analysis for idle speed control. A crank-angle domain viewpoint. *Proceedings of the American Control Conference, New Mexico*, June 1997; 278–283.

13. Yan Wang, Anna Stephanopoulou, Mike Levin. Idle speed control: An old problem in a new engine design. *Proceedings of the American Control Conference, San Diego*, 1999; 1217–1221.

14. Kiencke U, Nielsen L. *Automotive Control Systems*. Springer: Berlin, 2000.

15. Kang JM, Kolmanovsky I, Grizzle JW. Approximate dynamic programming solutions for lean burn engine aftertreatment. *IEEE Conference on Decision and Control, Phoenix, AZ*, 1999.

16. Sun J, Kolmanovsky I, Brehob D, Cook JA, Buckland J, Haghgooie M. Modeling and control of gasoline direct injection stratified charge (disc) engines. *International Conference on Control Applications*, 1999.

17. Cook JA, Powell BK. Discrete simplified external linearization and analytical comparison of IC engine families. *Proceedings of the American Control Conference, Minneapolis*, June 1987; 325–333.

18. Hendricks E, Chevalier A, Jensen M. Event based engine control: Practical problems and solutions. *SAE Paper* (950008), 1995.

19. Kolmanovsky I, Sun J, Druzhinina M, van Nieuwstadt M. Charge control for direct injection spark ignition engines with egr. *Proceedings of the American Control Conference, Chicago, IL*, 2000.

20. Verma R, Baskett I, Shah M, Maudie T, Mladenovic D, Sooriakumar K. A monolithic integrated solution for map applications. *SAE Paper* (970608), 1997.

21. ECM: Engine Control and Monitoring. AFRecorder 4800, Dual Channel Fast Air-to-Fuel Ratio Analyzer. *Instruction Manual*, 1999.

22. Yamada T, Hayakawa N, Kami Y, Kawai T. Universal air–fuel ratio heated exhaust gas oxygen sensor and further applications. *SAE Paper* (920234), 1992.

23. Ribbens W. *Understanding Automotive Electronics*. (5th edn). SAE International. Warrendale, PA, 1998.

24. Stefanopoulou AG, Butts KR, Cook JA, Freudenberg JS, Grizzle JW. Consequences of modular controller development for automotive powertrains: a case study. *Proceedings of IEEE Conference on Decision and Control, New Orleans*, December 1995; 768–773.

25. Buckland J, Grizzle JW. Idle speed control of a lean burn direct injection spark ignition engine. *Proceedings of the 5th International Symposium on Advanced Vehicle Control, Ann Arbor, MI*, August 2000; 205–212.

26. Yang M, Sorenson SC. Direct digital control of diesel engines. *SAE Paper* (940372), 1994.

27. Goodwin GC, Graebe SF, Salgado ME. *Control System Design*. Prentice-Hall: Englewood Cliffs, NJ, 2001.